ACSNANO

www.acsnano.org

ARTICLE

Enhanced Emission from Bright Excitons in Asymmetrically Strained Colloidal CdSe/$Cd_xZn_{1-x}Se$ Quantum Dots

Igor Fedin, Mateusz Goryca, Dan Liu, Sergei Tretiak, Victor I. Klimov,* and Scott A. Crooker*

Cite This: *ACS Nano* 2021, 15, 14444−14452

Read Online

ACCESS | Metrics & More | Article Recommendations | Supporting Information

ABSTRACT: **Colloidal CdSe quantum dots (QDs) designed with a high degree of asymmetric internal strain have recently been shown to host a number of desirable optical properties including subthermal room-temperature line widths, suppressed spectral diffusion, and high photoluminescence (PL) quantum yields. It remains an open question, however, whether they are well-suited for applications requiring emission of identical single photons. Here we measure the low-temperature PL dynamics and the polarization-resolved fluorescence line narrowing spectra from ensembles of these strained QDs. Our spectroscopy reveals the radiative recombination rates of bright and dark excitons, the relaxation rate between the two, and the energy spectra of the quantized acoustic phonons in the QDs that can contribute to relaxation processes. In comparison to conventional colloidal CdSe/ZnS core/shell QDs, we find that in asymmetrically strained CdSe QDs over six times more light is emitted directly by the bright exciton. These results are therefore encouraging for the prospects of chemically synthesized colloidal QDs as emitters of single indistinguishable photons.**

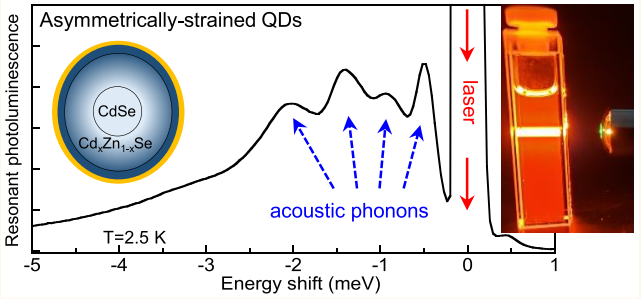

KEYWORDS: *nanocrystal, colloidal quantum dot, single-photon emitter, exciton fine structure, acoustic phonon, bright exciton*

INTRODUCTION

Semiconductor quantum dots (QDs) are a proven materials platform for applications requiring single-photon emission.[1,2] Furthermore, recent work has demonstrated significant progress toward the use of QDs as on-demand sources of single photons that are quantum mechanically indistinguishable (*i.e.*, identical in all degrees of freedom), an essential ingredient in many quantum communication and sensing proposals. Particular success has been achieved with self-assembled III−V QDs grown by molecular-beam epitaxy, especially when such QDs are integrated into photonic cavities that accelerate spontaneous exciton emission rates (*via* the Purcell effect) in comparison to exciton relaxation and dephasing rates that arise from undesired coupling to the surrounding environment (*e.g.*, phonons, electrostatic noise, local electronic and nuclear spin fluctuations, *etc.*).[3−6]

Colloidal semiconductor QDs made by synthetic chemistry, which feature widely tunable emission wavelength and high photoluminescence (PL) quantum yields, also perform very well as emitters of single photons.[7−13] However, achieving single-photon indistinguishability with colloidal QDs presents a more substantial challenge and has historically been hindered by spectral instability, emission intermittency (blinking), and fast exciton dephasing due to phonon coupling and interactions with surface defects, all of which limit their suitability for many quantum photonics applications. For example, intensity fluctuations in colloidal QDs are typically ascribed to random charging/discharging events, which in turn lead to activation/deactivation of nonradiative Auger recombination and fluctuating nonradiative decay channels.[14−17] Furthermore, spectral fluctuations are typically explained by interactions with the fluctuating electrostatic environment, which affects exciton energies through the Stark effect.[18,19] In this context, a noteworthy advance was the development of colloidal CdSe QDs with thick CdS shells,[20,21] which largely mitigated PL intermittency due to suppression of Auger recombination channels and improved isolation of the emitting exciton state from the fluctuating environment.

Received: May 6, 2021
Accepted: August 23, 2021
Published: September 2, 2021

https://doi.org/10.1021/acsnano.1c03864
ACS Nano 2021, 15, 14444−14452

More recently, a new class of asymmetrically strained colloidal QDs having CdSe cores enclosed by compositionally graded $Cd_xZn_{1-x}Se$ shells were shown to exhibit spectrally stable emission and subthermal line widths at room temperature.[22,23] These advantageous properties originate from the nearly ideal local charge neutrality of the emitting exciton state, that is, the nearly perfect spatial overlap of electron and hole envelope wave functions in the QD. This results in reduced coupling to polar vibrations (and hence, narrow line width) and suppressed interactions with external fluctuating charges (and, hence, stable emission wavelength). However, the suitability of these asymmetrically strained CdSe QDs as robust sources of identical photons has not been established, in part because their intrinsic radiative emission rates and nonradiative relaxation channels were not studied in detail. These critical properties depend on the interplay between the exciton's underlying fine structure (comprising optically allowed "bright" and nominally forbidden "dark" states) and the coupling of bright excitons to lattice vibrations (phonons), surface states (created by, for example, dangling bonds), and the surrounding electrostatic environment.[24−31]

To address these gaps, here we measure the temperature-dependent PL dynamics (*i.e.*, PL kinetics) and the polarization-resolved fluorescence line narrowing (FLN) spectra from ensembles of asymmetrically strained colloidal QDs. These studies reveal the bright and dark exciton states, their intrinsic radiative emission rates, the relaxation rate between the two states, and the energy spectra of the quantized acoustic phonons. Interestingly, the thermal activation of dark exciton PL occurs on energy scales of approximately 2−3 meV, which is substantially larger than the lowest-energy acoustic phonon modes of the QDs that are directly observed in FLN spectra. Most importantly, we find that in asymmetrically strained CdSe QDs the fraction of all light that is emitted directly by the bright exciton is considerably larger (accounting for 39% of all emitted photons) in comparison with conventional CdSe/ZnS core/shell colloidal QDs (6.4% of all emitted photons), which is very encouraging for their potential use as emitters of single indistinguishable photons.

RESULTS AND DISCUSSION

The inset of Figure 1a shows a schematic of the asymmetrically strained core/shell QDs studied in this work, which were synthesized by a multistep continuous-injection protocol developed recently.[22,32] Asymmetric compression of the wurtzite CdSe core is achieved by coating the core with a $Cd_xZn_{1-x}Se$ shell, where x is continuously graded from 1 at the core surface to 0 at the shell periphery (for this reason, hereinafter we refer to these structures as "cg-QDs"). Continuous grading avoids strain-relieving lattice defects and associated dangling bonds, and the nonuniform strain profile originates from the directionally asymmetric lattice mismatch between CdSe and ZnSe.[22] Additional thin shells of wide-gap $ZnSe_{0.5}S_{0.5}$ and ZnS are then grown to enhance QD stability (see Materials and Methods and also Supporting Information). These cg-QDs exhibit type-I band alignment, with both electron and hole strongly localized in the CdSe core. Figure 1a shows the absorption and PL spectra from a typical ensemble of these cg-QDs at room temperature. Asymmetric compression further increases the splitting between the heavy- and light-hole valence bands in the wurtzite CdSe core, leading to a characteristic double-peaked absorption of the band-edge exciton that is clearly resolvable even in ensemble spectra.[22,23]

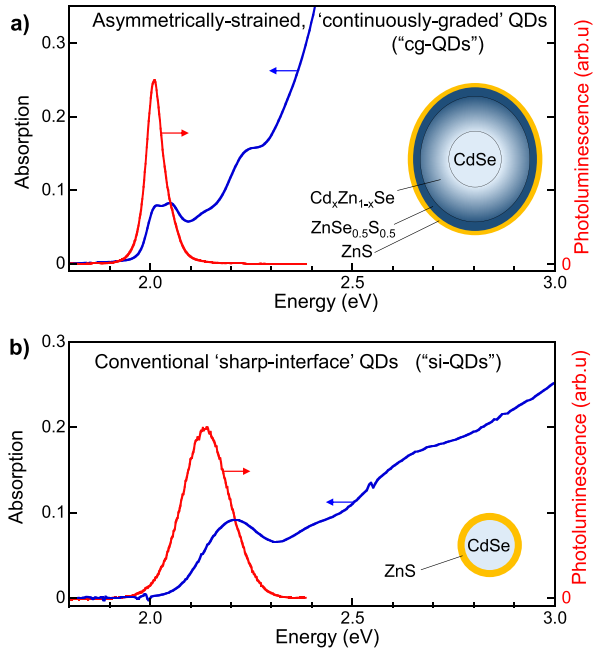

Figure 1. (a) Room-temperature absorption and photoluminescence (PL) spectra from asymmetrically strained, compositionally graded CdSe/$Cd_xZn_{1-x}Se$/$ZnSe_{0.5}S_{0.5}$/ZnS QDs ("cg-QDs"). The emitting wurtzite core is asymmetrically compressed due to anisotropic lattice mismatch with the surrounding shell. These cg-QDs have 5.2 nm diameter CdSe cores (on average) and ∼6 nm thick shells. (b) Room-temperature absorption and PL spectra of conventional CdSe/ZnS colloidal QDs that have a sharp interface between the core and shell ("si-QDs"). These CdSe cores have 3.4 nm diameters, and the ZnS shells are ∼1 nm thick.

For the purposes of direct comparison with the cg-QDs, we also perform the same measurements on reference ensembles of conventional CdSe/ZnS core/shell QDs. As depicted in Figure 1b, these QDs have a sharp interface between the CdSe core and the ZnS shell and are henceforth called "si-QDs". Figure 1b shows typical room-temperature absorption and PL spectra from these conventional si-QDs. Importantly, these si-QDs also exhibit type-I band alignment (in contrast to, for example, CdSe/CdS structures), and as shown below, they exhibit a similar bright−dark exciton splitting as cg-QDs, making them suitable control samples. Low-temperature PL spectra from both cg-QDs and the control si-QDs are shown in the Supporting Information.

For measurements at low temperatures, the QDs were prepared as high-optical-quality slabs of QD/PLMA composite [where PLMA is poly(lauryl methacrylate)] and were mounted in the variable-temperature insert of an optical cryostat. PLMA provides a "soft" host matrix and therefore a large acoustic impedance mismatch with the comparatively "stiff" QD, which improves the visibility of acoustic phonon modes as shown below. Nonresonant time-resolved PL measurements, and also fluorescence line narrowing studies, were performed at low temperatures down to 2.2 K (see Materials and Methods).

Figure 2 shows PL decays from both the cg-QDs and the control si-QDs. At low temperatures, we observe a fast initial drop, followed by a much slower decay on longer time scales. Qualitatively, low-temperature PL decays exhibiting an overall two-component relaxation are routinely observed for colloidal II−VI QDs.[33−40] In the opposite limit of high temperatures, the PL decays are monoexponential and largely independent of

https://doi.org/10.1021/acsnano.1c03864
ACS Nano 2021, 15, 14444−14452

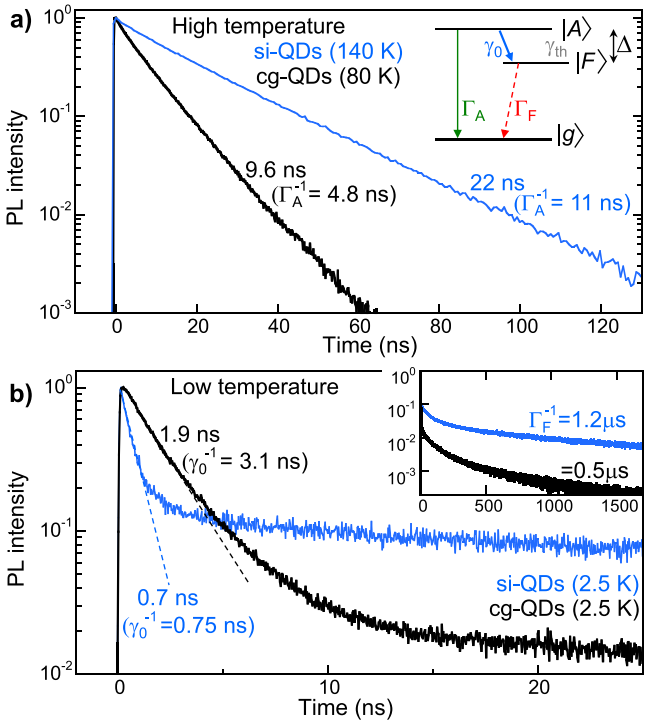

Figure 2. (a) Inset: Energy level diagram depicting the lowest optically allowed $|A\rangle$ and optically forbidden $|F\rangle$ exciton states (*i.e.*, the bright and dark excitons) and possible recombination/relaxation pathways. Main figure: Time-resolved PL decays, normalized by total area, from cg-QDs (black trace) and si-QDs (blue trace), at high temperature. The decays are monoexponential, from which the bright exciton radiative rate Γ_A can be determined (see main text). (b) Same, but at low temperature (2.5 K). The fast initial relaxation decays with a combined rate $\Gamma_A + \gamma_0$, where γ_0 is the zero-temperature bright−dark relaxation rate. The slow decay rate Γ_F from the forbidden dark exciton state is much longer compared to other rates. For cg-QDs and conventional si-QDs, the fraction of the total emission from bright excitons, $\Gamma_A/(\Gamma_A + \gamma_0)$, is 39% and 6.4%, respectively. This significant enhancement is due to the faster emission rate and the 4-fold reduction of γ_0 in the cg-QDs.

temperature. These behaviors can be rationalized by considering the underlying energy level structure (*i.e.*, the "fine structure") of the band-edge exciton.

As is very well established, the exciton fine structure in colloidal wurtzite CdSe QDs arises from the combined effects of the QD's crystal/shape anisotropy and the confinement-enhanced exchange interaction between the spin-1/2 electron and the angular-momentum-3/2 hole.[39,41−45] These effects lift the 8-fold degeneracy of the exciton, such that the lowest-energy exciton state has net angular momentum projection J along the QD's wurtzite $\hat{c}$ axis of either $J = \pm 2$ (for most quasi-spherical QDs) or $J = 0$ (for highly prolate or rod-like QDs). Both states are nominally forbidden from direct radiative recombination within the electric dipole approximation and are therefore optically "dark". Typically residing just a few millielectronvolts above this dark ground state exciton are optically allowed "bright" exciton states with $J = \pm 1$. The other exciton fine structure levels are higher in energy and therefore play a much smaller role in the PL dynamics.

The minimal energy level diagram from which the PL dynamics can be readily understood is shown in the inset of Figure 2a. Bright excitons in the lowest optically allowed level $|A\rangle$ can radiatively recombine with intrinsic radiative rate Γ_A. In contrast, dark excitons in the nominally forbidden state $|F\rangle$ at even lower energy can only undergo assisted radiative recombination, with much slower rate Γ_F. The energy separation between the bright and dark states is given by Δ and is related to electron−hole exchange, crystal field splitting, and shape anisotropy. Exciton relaxation and scattering from the bright to dark levels, captured here by the rate γ_0, requires a spin-flip of the electron or hole and is mediated by interactions with the environment in or surrounding the QD, typically by the coupling of excitons to low-energy acoustic phonon modes of the QD itself and to dangling bonds at the QD surface or at the core/shell interface(s). The zero-temperature relaxation rate γ_0 is an especially important parameter that, in general, one aims to minimize in single-photon emitters, since it represents a nonradiative relaxation/dephasing pathway for bright excitons. To maximize the amount of light that bright excitons can emit within their characteristic relaxation time, we therefore seek an ideal regime where $\gamma_0 \ll \Gamma_A$. (Note that in the diagram γ_{th} is a temperature-dependent rate that thermalizes bright and dark states at elevated temperatures; it vanishes in the limit of low temperature.)

The three-level model shown in Figure 2a is widely used to capture the essential trends of temperature-dependent PL dynamics in colloidal QDs.[34,35,37−39,46−49] Limiting-case behaviors can be readily understood: At very low temperatures, the slow PL decay rate on long time scales is given simply by Γ_F, while the faster initial decay is given by $\Gamma_A + \gamma_0$ (note that γ_{th} is negligible at low temperature). In the opposite limit of high temperatures, excitons are effectively thermalized across all bright and dark states, and the decays are monoexponential and independent of temperature, with an approximate rate $\Gamma_A/2$ (here we assume that bright and dark states have identical degeneracy factors).

For both the cg-QDs and the reference si-QDs, the rates Γ_A, Γ_F, and γ_0 can therefore be directly inferred from the PL dynamics in the high- and low-temperature limits. As shown in Figure 2a, the PL decays at high temperatures are indeed monoexponential as expected; however they are faster for the cg-QDs in comparison with the conventional si-QDs, in agreement with initial studies of these asymmetrically strained QDs.[22] From these monoexponential PL decays we determine the bright exciton decay rate $\Gamma_A^{cg} \simeq 0.21$ ns^{-1} (≃4.8 ns decay time) for the cg-QDs and $\Gamma_A^{si} \simeq 0.091$ ns^{-1} (≃11 ns decay time) for the si-QDs.

The PL decays at low temperatures (Figure 2b) exhibit very slow relaxation on long time scales from which we determine $\Gamma_F^{cg} \simeq 0.0021$ ns^{-1} (≃500 ns decay) for the cg-QDs and $\Gamma_F^{si} \simeq 0.0008$ ns^{-1} (≃1200 ns decay) for the si-QDs. These values are in line with many earlier studies of slow low-temperature PL dynamics from optically forbidden dark excitons in colloidal QDs.[33−40,49]

Most importantly, the rapid PL decays on *short* time scales at low temperatures, which decay with the rate $\Gamma_A + \gamma_0$ as discussed above, are nearly three times faster in the conventional si-QDs as compared to the strained cg-QDs. Crucially, from these initial decays (and the prior determination of Γ_A) we determine γ_0, the zero-temperature relaxation rate from bright to dark states. We find that $\gamma_0^{cg} = 0.32$ ns^{-1} (≃3.1 ns decay time) in the cg-QDs and a much faster $\gamma_0^{si} = 1.3$ ns^{-1} (≃0.75 ns decay time) in the reference si-QDs.

https://doi.org/10.1021/acsnano.1c03864
ACS Nano 2021, 15, 14444−14452

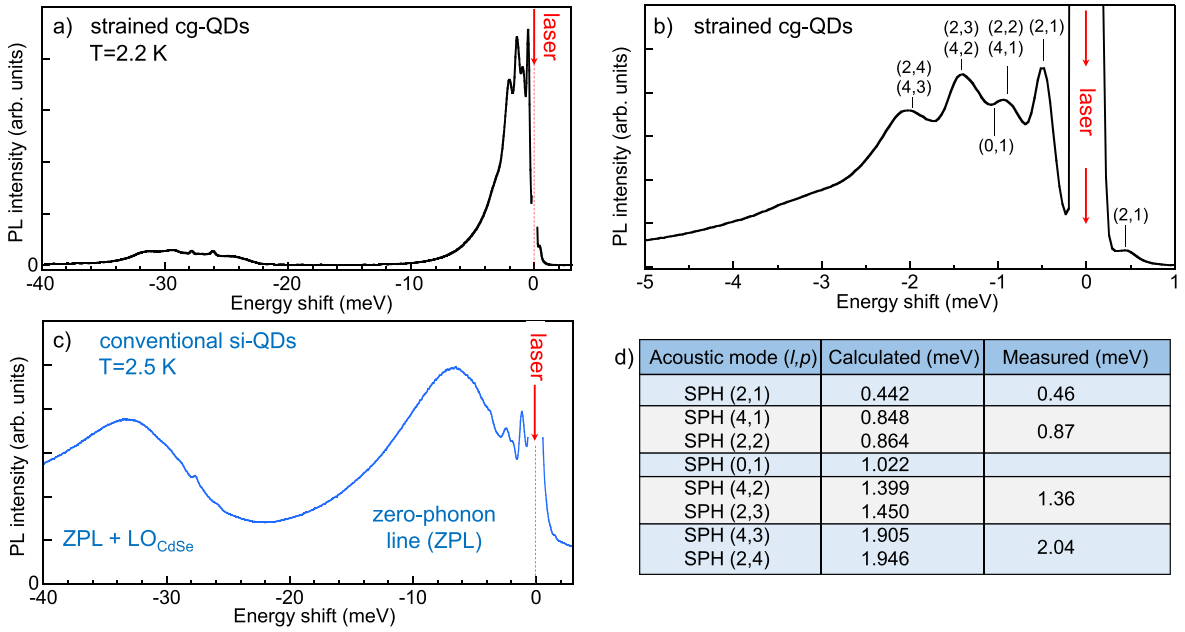

d)

Acoustic mode (l,p)	Calculated (meV)	Measured (meV)
SPH (2,1)	0.442	0.46
SPH (4,1)	0.848	0.87
SPH (2,2)	0.864	
SPH (0,1)	1.022	
SPH (4,2)	1.399	1.36
SPH (2,3)	1.450	
SPH (4,3)	1.905	2.04
SPH (2,4)	1.946	

Figure 3. (a) FLN spectrum of cg-QDs. The pump photon energy is 2.1017 eV. (b) Same, but on an expanded scale, showing quantized low-energy acoustic phonon modes. (c) FLN spectrum of conventional si-QDs. Dark exciton emission is much stronger. The pump photon energy is 2.1754 eV. (d) Comparing the calculated and measured acoustic phonon energies in the cg-QDs. A table of calculated and measured acoustic phonon energies for the control si-QDs and an expanded plot of the LO-phonon band in the cg-QDs are given in the Supporting Information.

This 4-fold difference in γ_0, together with the faster radiative recombination rate Γ_A, means that the fraction of all light emitted by the bright exciton, $\Gamma_A/(\Gamma_A + \gamma_0)$, is much larger in cg-QDs (39%) in comparison with the conventional si-QDs (6.4%), as shown in Figure 2b. This difference, which exceeds a factor of six, strengthens the potential of cg-QDs as single-photon emitters for quantum photonics.

Undesired relaxation and scattering from bright to dark exciton levels occurs *via* interaction with the environment, for example, by coupling of excitons to low-energy acoustic phonon modes of the QD itself or to unpassivated (dangling) bonds at core/shell interfaces or at the QD surface. Indeed, single-QD studies by Werschler *et al.*[40] demonstrated an increase of the bright−dark relaxation rate γ_0 when the bright−dark splitting was commensurate with a confined acoustic phonon energy. It is therefore important to measure and quantify the energy spectrum of acoustic phonons in our colloidal cg-QD and si-QD ensembles. To this end, we performed high-resolution FLN studies at low temperatures down to 2 K. The QD ensembles were resonantly pumped on the low-energy side of the band-edge exciton absorption peak using narrowband light from a cw tunable dye laser. Primarily, only a small subset of QDs having bright ($J = \pm 1^L$) exciton absorption energy exactly resonant with the pump laser were photoexcited,[50,51] and the quasi-resonant emission from this subset was detected with high spectral resolution.

Figure 3a shows a characteristic FLN spectrum from a cg-QD ensemble, plotted as a function of the energy shift from the resonant pump laser. The first longitudinal optical (LO) phonon replica region is seen at large energy shifts (25−35 meV); it contains LO-phonon-assisted emission from bright and dark excitons as well as emission due to the combination of LO phonons and various low-energy acoustic phonons.

Crucially, Figure 3b shows an expanded plot of the same FLN spectrum at small energy shifts, which reveals a highly structured emission containing multiple sharp peaks at very small energy shifts of only a few meV or less. The lowest-energy peak lies only 0.46 meV away from the pump laser, followed by additional peaks at 0.87, 1.36, and 2.04 meV. As discussed below, these peaks correspond to the calculated energies of the quantized acoustic phonon (vibrational) modes of the cg-QDs. Their visibility in the ensemble FLN spectrum derives from the high degree of acoustic impedance mismatch between the QDs and the comparatively "soft" surrounding PLMA composite. This allows us to consider the QDs as elastic spheres with free (unclamped) boundaries and use a standard Lamb theory[52] to calculate the energies of the expected acoustic phonon modes in these QDs.

Within Lamb's model, acoustic modes of a homogeneous sphere are characterized as spheroidal or torsional and are described by the angular and principal quantum numbers (l, p), where l is the number of angular nodes and $p - 1$ is the number of radial nodes. Typically, only the spheriodal modes couple to electronic transitions.[25,53] A complete solution of the mode energies, particularly as applied to spherical semiconductor quantum dots, depends on the transverse and longitudinal sound speeds in the material and has been discussed broadly in the literature.[25,51,53−58] The energies of all (l, p) modes scale inversely with the total diameter of the quantum dot. We model these cg-QDs as uniform elastic spheres with 16 nm net diameter, which corresponds closely to the typical dimensions of these cg-QDs and composition-weighted average longitudinal and transverse sound velocities of 4.41 and 2.03 km/s, respectively. Using these values we calculate that the lowest-energy spheroidal vibration is the (2,1) mode with energy 0.44 meV. The next $l = 2$ spheroidal mode is (2,2) with energy 0.85 meV [this mode is nearly degenerate with the spheroidal (4,1) mode]. These calculated energies correspond closely to the experimentally measured values of 0.46 and 0.87 meV, respectively. Figure 3d shows a

https://doi.org/10.1021/acsnano.1c03864
ACS Nano 2021, 15, 14444−14452

more complete comparison of measured and calculated values. Interestingly, the calculated energy of the lowest $l = 0$ spheroidal mode, which is the (0,1) pure breathing mode, is 1.022 meV, for which the data do not clearly evince a discrete peak. Overall, these data concur very well with the series of $l = 2$ discrete acoustic phonon modes [and also the absence of any clear (0,1) mode] that was observed in studies of single CdSe/CdS/PMMA nanoparticles by Werschler *et al.*[40]

In comparison, Figure 3c shows a FLN spectrum from the reference ensemble of si-QDs, which were also embedded in PLMA. This FLN spectrum is characteristic of conventional CdSe QDs,[30,47,50,51,59] in that it shows a broad and well-resolved emission peak that is clearly separated from the pump laser (by about 7 meV in this case), along with its strong CdSe LO phonon replica located ~26 meV lower in energy. Following the usual interpretation, the broad peak at 7 meV is associated with the "zero-phonon line" from dark excitons; however this peak may be further red-shifted at these low temperatures by magnetic polaron-like effects arising from dangling bonds at the core−shell interface or QD surface.[30] Temperature-dependent FLN spectra of these si-QDs do indicate a red-shift with decreasing temperature (Supporting Information). At small energy shifts (<3 meV), additional sharp peaks corresponding to discrete acoustic phonon modes are observed. As discussed above, their visibility in ensemble spectra is likely due to the acoustic isolation provided by the surrounding PLMA composite. The two most prominent peaks are 1.16 and 2.45 meV away from the pump laser. Assuming these si-QDs have net diameters of 5.8 nm (corresponding to 3.4 nm diameter cores and 1.2 nm thick shells), these values are in quite reasonable agreement with the calculated energy of the lowest energy spheroidal (2,1) mode of 1.25 meV, and the energies of the nearly degenerate (2,2) and (4,1) acoustic modes (2.40 and 2.45 meV, respectively).

It is evident from Figure 3a and c that asymmetrically strained cg-QDs exhibit markedly different FLN spectra as compared to conventional si-QDs. Most notably, the ratio of dark exciton emission intensity in comparison to the acoustic phonon replicas from the resonantly pumped $J = \pm 1^L$ bright excitons is much smaller in cg-QDs. Indeed, signatures of dark exciton emission in the FLN spectrum from the cg-QDs are not immediately apparent in Figure 3a,b, because they are weak and are obscured by the much stronger acoustic phonon replicas of the bright exciton. This difference in FLN spectra is qualitatively consistent with the marked difference in their PL dynamics (discussed above, *cf.* Figure 2), where cg-QDs were found to emit over six times more light from bright excitons in comparison with si-QDs.

At this point it is natural to ask whether the acoustic phonon energies directly measured by FLN are related to the activation energy that is commonly inferred from the temperature dependence of the long-lived PL lifetime. It is well established that the slow PL lifetime from colloidal QDs accelerates significantly with increasing temperature.[34,35,37,49] In early experiments, this variation was usually ascribed to the thermal activation of long-lived dark excitons to the higher-lying short-lived bright levels, a consequence of the exciton fine structure and the energy splitting Δ between the lowest dark and bright states. However, the measured activation energies deduced from temperature-dependent PL lifetimes studies were typically much smaller (only 1−5 meV, depending on QD size) than the expected bright−dark splittings Δ (2−20 meV, depending on the QDs' size).[34,37,49] These findings prompted suggestions that the relevant activation energy scale might instead be related to interactions with dangling bonds[34] or with the quantized acoustic phonon modes of the QDs themselves.[37,46,47,60] Studies of different QD sizes have shown an appealing correlation between the measured activation energies and the calculated acoustic phonon energies.[37,46,60]

We therefore compare our directly measured acoustic phonon energies with the activation energy inferred from temperature-dependent PL (Figure 4). In accordance with past

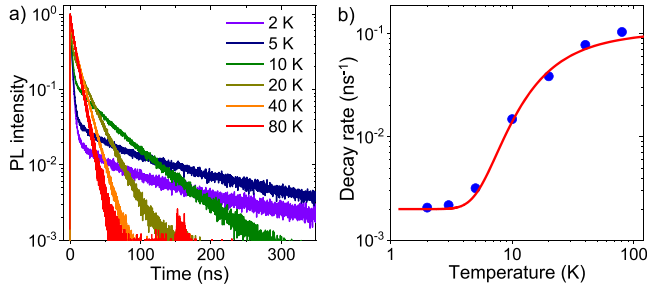

Figure 4. (a) PL decays from cg-QDs at different temperatures. (b) Measured decay rate of the long-lived PL decay *vs* temperature (points). Red line shows a fit to the data, from which a characteristic activation energy can be inferred. Corresponding fits to the si-QDs are shown in the Supporting Information.

works, here we assume only a thermal (Boltzmann) distribution of excitons between a long-lived dark state (with slow radiative rate Γ_F) and a higher-lying fast state (with fast radiative rate Γ_A). As derived previously,[34,37,49] in this case the net PL decay rate Γ can be expressed as $\Gamma = (\Gamma_F + e^{-\beta E}\Gamma_A)/(1 + e^{-\beta E})$, where E is the activation energy and $\beta^{-1} = k_B T$ is the thermal energy. Interestingly, these temperature-dependent lifetimes reveal an activation energy $E \simeq 2.4$ meV, which substantially exceeds the measured energy of the lowest (2,1) and (2,2) acoustic phonon modes in these cg-QDs and also the (0,1) acoustic breathing mode. For the si-QDs, a similar analysis of PL lifetimes yields $E \simeq 3.0$ meV, which again exceeds the lowest ($l = 2$) acoustic phonon modes discussed above, but is roughly commensurate with the expected (0,1) mode in QDs of this size (see Supporting Information for details). While consideration of acoustic phonon coupling to excitons is undoubtedly important for the photophysics of colloidal QDs,[24,27,61] our direct experimental comparison between thermal activation energies and measured acoustic phonon energies indicates that the lowest-energy vibrational modes of QDs may not always represent a principal activation pathway.

Returning to FLN spectra, we highlight two additional noteworthy aspects. The first is that evidence for dark excitons in the cg-QDs can be observed by scanning the resonant pump laser through the ensemble's broad band-edge absorption peak. Tuning the pump laser to lower/higher photon energy preferentially photoexcites subsets of QDs with slightly larger/smaller CdSe cores, respectively. The core size determines the confinement and therefore the electron−hole exchange energy, which in turn affects the bright−dark splitting.[41,42] Figure 5a and b show examples of FLN spectra and the measured energies of the FLN peaks as the pump laser energy is varied. Low-energy acoustic phonon energies change very little, because their energies are determined by the overall size of the QD (core + thick graded shell). However, the

https://doi.org/10.1021/acsnano.1c03864
ACS Nano 2021, 15, 14444−14452

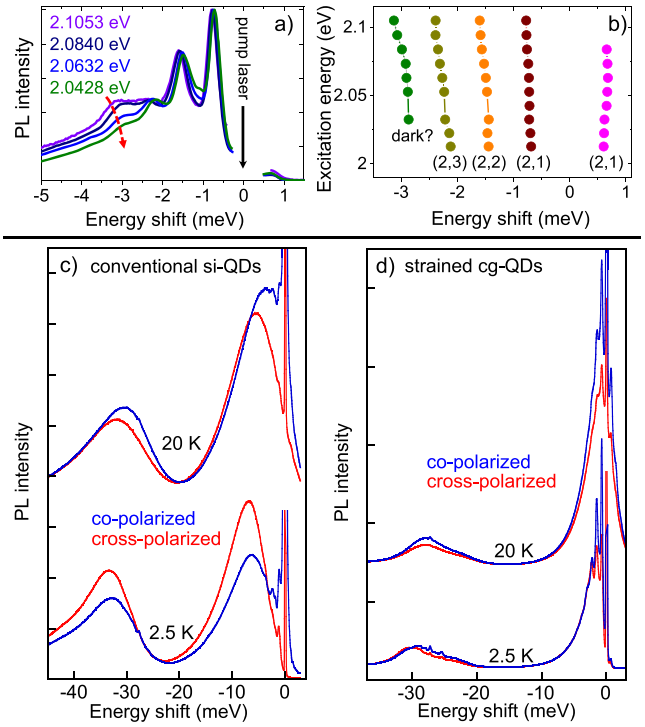

Figure 5. (a) FLN spectra of a cg-QD ensemble, at different resonant pump laser energies indicated in the legend, at T = 2.5 K. (Note: these cg-QDs have a smaller net radius than those studied in Figure 3 and therefore larger phonon energies.) (b) Extracted energy shifts of the FLN peaks (x-axis) as the photon energy of the pump laser (y-axis) is varied. (c) Co- and crossed-polarized FLN spectra from conventional si-QDs. At 2.5 K, dark exciton PL (and its LO-phonon replica) are polarized orthogonal to the bright ($J = \pm 1^L$) exciton that is resonantly excited by the linearly polarized pump laser. By 20 K, the emission becomes collinearly polarized. (d) Same, but for cg-QDs. Preferentially cross-polarized emission is barely evident, except for the lowest temperatures and at the largest energy shift.

spectra do show a peak that shifts noticeably with pump photon energy, in the range of approximately 3 meV. We tentatively identify this peak with dark exciton emission in the cg-QDs. We note that a related analysis was recently performed on CdSe/CdS dot-in-rods.[62] This dark exciton energy is less than the zero phonon line energy observed in si-QDs, but this difference is strongly influenced by a greatly reduced coupling to dangling bonds in cg-QDs (and consequent magnetic polaron effects), because the graded core−shell interface reduces the number of defects and dangling bonds.

A second noteworthy aspect is the dependence of the FLN spectra on linear polarization. In conventional si-QDs, at very low temperatures (2.5 K), quasi-resonant PL detected with linear polarization orthogonal (crossed) to the pump laser polarization is substantially larger than for the case of collinear detection, for both the dark exciton emission and its optical phonon replica (see Figure 5c). However, by 20 K the effect is reversed, and the co-polarized FLN spectrum is more intense than the cross-polarized spectrum. This interesting behavior, which was also inferred in early studies of conventional colloidal QDs,[42,51] is related to the underlying mechanisms of dark exciton emission. As discussed recently by Rodina and Efros,[61] emission from dark states can be cross- or collinearly polarized (with respect to the $J = \pm 1^L$ bright exciton dipole that was resonantly pumped), depending on whether the emission was assisted by phonons or by dangling bonds, respectively. These FLN spectra of si-QDs suggest that phonon-assisted mechanisms dominate at the lowest temperatures. In contrast, however, such a marked temperature variation is much less evident in the FLN spectra from cg-QDs (Figure 5d), where cross-linear emission is only very slightly larger at 2.5 K at the largest energy shifts. This behavior is again consistent with greatly reduced emission from dark excitons (in comparison to bright excitons) in the cg-QDs, as initially revealed by the PL decays shown in Figure 2 and by the much smaller value of γ_0 that was revealed in cg-QDs.

Taken together, both the low-temperature PL decays and the detailed FLN spectra indicate that asymmetrically strained cg-QDs emit over six times more light from bright excitons, in comparison with conventional si-QDs. This difference is attributed to the much slower bright−dark relaxation rate γ_0 in cg-QDs and their faster bright exciton radiative rate Γ_A. The latter results from the asymmetric strain on the CdSe core, which further separates valence band levels and increases the oscillator strength of the $J = \pm 1^L$ bright exciton transition dipole.[41] In this regard, future spectroscopic studies of single cg-QDs, particularly in applied magnetic fields, should help to identify the nature and energy structure of the exciton levels. Both cg-QDs as well as conventional si-QDs exhibit bright−dark splittings that exceed the lowest acoustic phonon energies in the nanocrystals, and thus it is not clear that the coupling of bright excitons to acoustic phonons should be markedly different in the two classes of QDs. On the other hand, coupling of excitons to dangling bonds and to a fluctuating electrostatic environment is greatly reduced in cg-QDs as compared to si-QDs, not only because of the local charge neutrality of the exciton itself but also because the continuously graded shell mitigates the formation of lattice defects, charge traps, and unpassivated bonds near the exciton wave function in the CdSe core. In these studies, it is difficult to gauge the importance of dangling bonds in the cg-QDs and their role in bright−dark exciton relaxation, precisely because the dark exciton emission is so weak in FLN spectra (in comparison to si-QDs). Once again, detailed polarization-resolved studies in high magnetic fields should provide critical insight.

CONCLUSIONS

In summary, our measurements demonstrate that bright excitons in cg-QDs emit much more light (39%), in comparison to ensembles of conventional core/shell si-QDs (6.4%). This marked enhancement derives from the enhanced emission rate and the 4-fold suppression of the bright−dark relaxation rate γ_0 in cg-QDs, which is due to a suppressed coupling to environmental fluctuations. This enhancement bodes well for their future promise as sources of quantum mechanically indistinguishable single photons, where each photon is emitted from the same unperturbed bright exciton state in the QD. Interferometric measurements will of course be necessary to confirm this possibility. Additional enhancement of the bright exciton emission in cg-QDs may be possible by incorporating them into photonic structures and cavities that further accelerate radiative recombination due to the Purcell effect and which can be tuned to suppress nonresonant emission modes, as demonstrated previously for epitaxially grown QDs.

https://doi.org/10.1021/acsnano.1c03864
ACS Nano 2021, 15, 14444−14452

MATERIALS AND METHODS

Materials and Synthesis. Asymmetrically strained and compositionally graded colloidal CdSe/$Cd_xZn_{1-x}Se$/$ZnSe_{0.5}S_{0.5}$/ZnS QDs were chemically synthesized by a continuous-injection protocol described recently by Kozlov *et al.*[32] and as detailed in the Supporting Information. The continuously graded $Cd_xZn_{1-x}Se$ shell mitigates strain-relieving lattice defects and dangling bonds near the CdSe core and also provides the asymmetric strain profile on the CdSe core due to the directionally asymmetric lattice mismatch between CdSe and ZnSe. For synthesis of the conventional sharp-interface CdSe/ZnS QDs, care was taken to avoid any compositional grading. Therefore, we synthesized stoichiometric wurtzite CdSe cores and overgrew ZnS shells using very reactive Zn and S precursors $Zn(C_2H_5)_2$ and $[(CH_3)_3Si]_2S$. Room-temperature PL and absorption spectra were obtained on liquid solutions of these QDs. For optical spectroscopy studies at low temperature, the QDs were prepared as high optical quality PLMA composites. In washing the QDs, we aimed to remove excess precursors from the QDs but keep surface ligands intact, so as to provide a "soft" acoustic interface between the QDs and the PLMA, which allows us to consider the QDs as elastic spheres with free boundary conditions.

Time-Resolved Photoluminescence. The QD-PLMA composite samples were mounted in the variable-temperature insert (2−300 K) of a helium cryostat with direct optical access. Nonresonant time-resolved PL was measured by time-correlated single-photon counting, using 80 ps pulses from a 3.1 eV pulsed diode laser as the excitation source. The excitation was very weak (<50 μW average power, ∼1 mm spot diameter), corresponding to the subsingle exciton/QD regime, as indicated by the lack of biexciton signatures in the PL dynamics. The emitted PL was spectrally dispersed in a 500 mm spectrometer and detected by a multichannel plate photomultiplier tube. Only a narrow (∼1 nm wide) band at the PL peak was used to measure the PL decays. The net instrument response time was approximately 100 ps.

Fluorescence Line Narrowing. Also known as "resonant PL", FLN measurements were performed using a continuous-wave narrowband dye laser as a tunable excitation source, at temperatures down to 2.2 K. As above, the excitation light had low average power and was weakly focused on the sample (<500 μW, ∼1 mm spot diameter). Excitation and detection beam paths were separated by approximately 10 degrees, so as to avoid collection of the specularly reflected excitation light. Polarization optics in both the excitation and detection beam paths allowed to detect co- and crossed-linear configurations. The emitted PL was dispersed in the same 500 mm spectrometer and detected by a liquid-nitrogen-cooled charge-coupled device.

ASSOCIATED CONTENT

Supporting Information

The Supporting Information is available free of charge at https://pubs.acs.org/doi/10.1021/acsnano.1c03864.

Details of QD synthesis; low-temperature PL spectra; temperature-dependent FLN spectra; additional analysis of time resolved PL data (PDF)

AUTHOR INFORMATION

Corresponding Authors

Victor I. Klimov − *Chemistry Division, Los Alamos National Laboratory, Los Alamos, New Mexico 87545, United States;* orcid.org/0000-0003-1158-3179; Email: klimov@lanl.gov

Scott A. Crooker − *National High Magnetic Field Lab, Los Alamos National Laboratory, Los Alamos, New Mexico 87545, United States;* orcid.org/0000-0001-7553-4718; Email: crooker@lanl.gov

Authors

Igor Fedin − *Chemistry Division, Los Alamos National Laboratory, Los Alamos, New Mexico 87545, United States; Department of Chemistry and Biochemistry, University of Alabama, Tuscaloosa, Alabama 35487, United States*

Mateusz Goryca − *National High Magnetic Field Lab, Los Alamos National Laboratory, Los Alamos, New Mexico 87545, United States;* orcid.org/0000-0001-7582-1880

Dan Liu − *Theory Division, Los Alamos National Laboratory, Los Alamos, New Mexico 87545, United States*

Sergei Tretiak − *Theory Division, Los Alamos National Laboratory, Los Alamos, New Mexico 87545, United States;* orcid.org/0000-0001-5547-3647

Complete contact information is available at: https://pubs.acs.org/10.1021/acsnano.1c03864

Funding

We gratefully acknowledge support from the Laboratory Directed Research and Development (LDRD) program at Los Alamos National Laboratory under project 20200213DR. The NHMFL is supported by National Science Foundation (NSF) Grant No. DMR-1644779, the State of Florida, and the U.S. Department of Energy.

Notes

The authors declare no competing financial interest.

REFERENCES

(1) Senellart, P.; Solomon, G.; White, A. High-Performance Semiconductor Quantum-Dot Single-Photon Sources. *Nat. Nanotechnol.* **2017**, *12*, 1026−1039.

(2) Aharonovich, I.; Englund, D.; Toth, M. Solid-State Single-Photon Emitters. *Nat. Photonics* **2016**, *10*, 631−641.

(3) Ding, X.; He, Y.; Duan, Z.-C.; Gregersen, N.; Chen, M.-C.; Unsleber, S.; Maier, S.; Schneider, C.; Kamp, M.; Höfling, S.; Lu, C.-Y.; Pan, J.-W. On-Demand Single Photons with High Extraction Efficiency and Near-Unity Indistinguishability from a Resonantly Driven Quantum Dot in a Micropillar. *Phys. Rev. Lett.* **2016**, *116*, 020401.

(4) Somaschi, N.; Giesz, V.; De Santis, L.; Loredo, J. C.; Almeida, M. P.; Hornecker, G.; Portalupi, S. L.; Grange, T.; Antón, C.; Demory, J.; Gomez, C.; Sagnes, I.; Lanzillotti-Kimura, N. D.; Lemaitre, A.; Auffeves, A.; White, A. G.; Lanco, L.; Senellart, P. Near-Optimal Single-Photon Sources in the Solid State. *Nat. Photonics* **2016**, *10*, 340−345.

(5) Müller, M.; Bounouar, S.; Jöns, K. D.; Glässl, M.; Michler, P. On-Demand Generation of Indistinguishable Polarization-Entangled Photon Pairs. *Nat. Photonics* **2014**, *8*, 225−228.

(6) Grange, T.; Somaschi, N.; Antón, C.; De Santis, L.; Coppola, G.; Giesz, V.; Lemaître, A.; Sagnes, I.; Auffèves, A.; Senellart, P. Reducing Phonon-Induced Decoherence in Solid-State Single-Photon Sources with Cavity Quantum Electrodynamics. *Phys. Rev. Lett.* **2017**, *118*, 253602.

(7) Michler, P.; Imamoglu, A.; Mason, M. D.; Carson, P. J.; Strouse, G. F.; Buratto, S. K. Quantum Correlation Among Photons from a Single Quantum Dot at Room Temperature. *Nature* **2000**, *406*, 968−970.

(8) Park, Y.-S.; Guo, S.; Makarov, N. S.; Klimov, V. I. Room Temperature Single-Photon Emission from Individual Perovskite Quantum Dots. *ACS Nano* **2015**, *9*, 10386−10393.

(9) Lin, X.; Dai, X.; Pu, C.; Deng, Y.; Niu, Y.; Tong, L.; Fang, W.; Jin, Y.; Peng, X. Electrically-Driven Single-Photon Sources Based On Colloidal Quantum Dots with Near-Optimal Antibunching at Room Temperature. *Nat. Commun.* **2017**, *8*, 1132.

(10) Utzat, H.; Sun, W.; Kaplan, A. E. K.; Krieg, F.; Ginterseder, M.; Spokoyny, B.; Klein, N. D.; Shulenberger, K. E.; Perkinson, C. F.; Kovalenko, M. V.; Bawendi, M. G. Coherent Single-Photon Emission

from Colloidal Lead Halide Perovskite Quantum Dots. *Science* **2019**, *363*, 1068−1072.
(11) Ihara, T.; Miki, S.; Yamada, T.; Kaji, T.; Otomo, A.; Hosako, I.; Terai, H. Superior Properties in Room-Temperature Colloidal-Dot Quantum Emitters Revealed by Ultralow-Dark-Count Detections of Temporally-Purified Single Photons. *Sci. Rep.* **2019**, *9*, 15941.
(12) Morozov, S.; Pensa, E. L.; Khan, A. H.; Polovitsyn, A.; Cortés, E.; Maier, S. A.; Vezzoli, S.; Moreels, I.; Sapienza, R. Electrical Control of Single-Photon Emission in Highly Charged Individual Colloidal Quantum Dots. *Sci. Adv.* **2020**, *6*, No. eabb1821.
(13) Saxena, A.; Chen, Y.; Ryou, A.; Sevilla, C. G.; Xu, P.; Majumdar, A. Improving Indistinguishability of Single Photons from Colloidal Quantum Dots Using Nanocavities. *ACS Photonics* **2019**, *6*, 3166−3173.
(14) Efros, Al. L.; Rosen, M. Random Telegraph Signal in the Photoluminescence Intensity of a Single Quantum Dot. *Phys. Rev. Lett.* **1997**, *78*, 1110−1113.
(15) Tang, J.; Marcus, R. A. Mechanisms of Fluorescence Blinking in Semiconductor Nanocrystal Quantum Dots. *J. Chem. Phys.* **2005**, *123*, 054704.
(16) Galland, C.; Ghosh, Y.; Steinbruck, A.; Sykora, M.; Hollingsworth, J. A.; Klimov, V. I.; Htoon, H. Two Types of Luminescence Blinking Revealed by Spectroelectrochemistry of Single Quantum Dots. *Nature* **2011**, *479*, 203−207.
(17) Yuan, G.; Gómez, D. E.; Kirkwood, N.; Boldt, K.; Mulvaney, P. Two Mechanisms Determine Quantum Dot Blinking. *ACS Nano* **2018**, *12*, 3397−3405.
(18) Empedocles, S. A.; Bawendi, M. G. Quantum-Confined Stark Effect in Single CdSe Nanocrystallite Quantum Dots. *Science* **1997**, *278*, 2114−2117.
(19) Empedocles, S. A.; Norris, D. J.; Bawendi, M. G. Photoluminescence Spectroscopy of Single CdSe Nanocrystallite Quantum Dots. *Phys. Rev. Lett.* **1996**, *77*, 3873−3876.
(20) Mahler, B.; Spinicelli, P.; Buil, S.; Quelin, X.; Hermier, J.-P.; Dubertret, B. Towards Non-Blinking Colloidal Quantum Dots. *Nat. Mater.* **2008**, *7*, 659−664.
(21) Chen, Y.; Vela, J.; Htoon, H.; Casson, J. L.; Werder, D. J.; Bussian, D. A.; Klimov, V. I.; Hollingsworth, J. A. Giant" Multishell CdSe Nanocrystal Quantum Dots with Suppressed Blinking. *J. Am. Chem. Soc.* **2008**, *130*, 5026−5027.
(22) Park, Y.-S.; Lim, J.; Klimov, V. I. Asymmetrically Strained Quantum Dots with Non-Fluctuating Single-Dot Emission Spectra and Subthermal Room-Temperature Linewidths. *Nat. Mater.* **2019**, *18*, 249−255.
(23) Lim, J.; Park, Y.-S.; Klimov, V. I. Optical Gain in Colloidal Quantum Dots Achieved With Direct-Current Electrical Pumping. *Nat. Mater.* **2018**, *17*, 42−49.
(24) Takagahara, T. Electron-Phonon Interactions and Excitonic Dephasing in Semiconductor Nanocrystals. *Phys. Rev. Lett.* **1993**, *71*, 3577−3580.
(25) Takagahara, T. Electron-Phonon Interactions in Semiconductor Nanocrystals. *J. Lumin.* **1996**, *70*, 129−143.
(26) Sagar, D. M.; Cooney, R. R.; Sewall, S. L.; Dias, E. A.; Barsan, M. M.; Butler, I. S.; Kambhampati, P. Size Dependent, State-Resolved Studies of Exciton-Phonon Couplings in Strongly Confined Semiconductor Quantum Dots. *Phys. Rev. B: Condens. Matter Mater. Phys.* **2008**, *77*, 235321.
(27) Huxter, V.; Scholes, G. D. Acoustic Phonon Strain Induced Mixing of the fine Structure in Colloidal CdSe Quantum Dots Observed by a Polarization Grating Technique. *J. Chem. Phys.* **2010**, *132*, 104506.
(28) Masia, F.; Accanto, N.; Langbein, W.; Borri, P. Spin-Flip Limited Exciton Dephasing in CdSe/ZnS Colloidal Quantum Dots. *Phys. Rev. Lett.* **2012**, *108*, 087401.
(29) Liu, A.; Almeida, D. B.; Bae, W.-K.; Padhila, L. A.; Cundiff, S. T. Simultaneous Existence of Confined and Delocalized Vibrational Modes in Colloidal Quantum Dots. *J. Phys. Chem. Lett.* **2019**, *10*, 6144−6150.
(30) Biadala, L.; Shornikova, E. V.; Rodina, A. V.; Yakovlev, D. R.; Siebers, B.; Aubert, T.; Nasilowski, M.; Hens, Z.; Dubertret, B.; Efros, A. L.; Bayer, M. Magnetic Polaron on Dangling-Bond Spins in CdSe Colloidal Nanocrystals. *Nat. Nanotechnol.* **2017**, *12*, 569−574.
(31) Walsh, B. R.; Sonnichsen, C.; Mack, T. G.; Saari, J. I.; Krause, M. M.; Nick, R.; Coe-Sullivan, S.; Kambhampati, P. Excited State Phononic Processes in Semiconductor Nanocrystals Revealed by Excitonic State-Resolved Pump/Probe Spectroscopy. *J. Phys. Chem. C* **2019**, *123*, 3868.
(32) Kozlov, O. V.; Park, Y.-S.; Roh, J.; Fedin, I.; Nakotte, T.; Klimov, V. I. Sub-Single-Exciton Lasing Using Charged Quantum Dots Coupled to a Distributed Feedback Cavity. *Science* **2019**, *365*, 672−675.
(33) Nirmal, M.; Norris, D. J.; Kuno, M.; Bawendi, M. G.; Efros, A. L.; Rosen, M. Observation of the 'Dark Exciton' in CdSe Quantum Dots. *Phys. Rev. Lett.* **1995**, *75*, 3728−3731.
(34) Crooker, S. A.; Barrick, T.; Hollingsworth, J.; Klimov, V. I. Multiple Temperature Regimes of Radiative Decay in CdSe Quantum Dots: Intrinsic Limits to the Dark-Exciton Lifetime. *Appl. Phys. Lett.* **2003**, *82*, 2793−2795.
(35) Labeau, O.; Tamarat, P.; Lounis, B. Temperature Dependence of the Luminescence Lifetime of Single CdSe/ZnS Quantum Dots. *Phys. Rev. Lett.* **2003**, *90*, 257404.
(36) Furis, M.; Hollingsworth, J. A.; Klimov, V. I.; Crooker, S. A. Time- and Polarization-Resolved Optical Spectroscopy of Colloidal CdSe Nanocrystal Quantum Dots in High Magnetic Fields. *J. Phys. Chem. B* **2005**, *109*, 15332−15338.
(37) Oron, D.; Aharoni, A.; Donega, C. d. M.; van Rijssel, J.; Meijerink, A.; Banin, U. Universal Role of Discrete Acoustic Phonons in the Low-Temperature Optical Emission of Colloidal Quantum Dots. *Phys. Rev. Lett.* **2009**, *102*, 177402.
(38) Biadala, L.; Louyer, Y.; Tamarat, Ph.; Lounis, B. Direct Observation of the Two Lowest Exciton Zero-Phonon Modes in Single CdSe/ZnS Nanocrystals. *Phys. Rev. Lett.* **2009**, *103*, 037404.
(39) Fernée, M. J.; Tamarat, P.; Lounis, B. Cryogenic Single-Nanocrystal Spectroscopy: Reading the Spectral Fingerprint of Individual Quantum Dots. *J. Phys. Chem. Lett.* **2013**, *4*, 609−618.
(40) Werschler, F.; Hinz, C.; Froning, F.; Gumbsheimer, P.; Haase, J.; Negele, C.; de Roo, T.; Mecking, S.; Leitenstorfer, A.; Seletskiy, D. V. Coupling of Excitons and Discrete Acoustic Phonons in Vibrationally Isolated Quantum Emitters. *Nano Lett.* **2016**, *16*, 5861−5865.
(41) Efros, A. L.; Rosen, M.; Kuno, M.; Nirmal, M.; Norris, D. J.; Bawendi, M. Band-Edge Exciton in Quantum Dots of Semiconductors with a Degenerate Valence Band: Dark and Bright Exciton States. *Phys. Rev. B: Condens. Matter Mater. Phys.* **1996**, *54*, 4843−4856.
(42) Chamarro, M.; Gourdon, C.; Lavallard, P.; Lublinskaya, O.; Ekimov, A. I. Enhancement of Electron-Hole Exchange Interaction in CdSe Nanocrystals: A Quantum Confinement Effect. *Phys. Rev. B: Condens. Matter Mater. Phys.* **1996**, *53*, 1336−1342.
(43) Gupalov, S. V.; Ivchenko, E. L. The Fine Structure of Excitonic Levels in CdSe Nanocrystals. *Phys. Solid State* **2000**, *42*, 2030−2038.
(44) Le Thomas, N.; Herz, E.; Schops, O.; Woggon, U.; Artemyev, M. V. Exciton Fine Structure in Single CdSe Nanorods. *Phys. Rev. Lett.* **2005**, *94*, 016803.
(45) Zhao, Q.; Graf, P. A.; Jones, W. B.; Franceschetti, A.; Li, J.; Wang, L.-W.; Kim, K. Shape Dependence of Band-Edge Exciton Fine Structure in CdSe Nanocrystals. *Nano Lett.* **2007**, *7*, 3274−3280.
(46) Eilers, J.; van Hest, J.; Meijerink, A.; Donega, C. d. M. Unravelling the Size and Temperature Dependence of Exciton Lifetimes in Colloidal ZnSe Quantum Dots. *J. Phys. Chem. C* **2014**, *118*, 23313−23319.
(47) Brodu, A.; Ballottin, M. V.; Buhot, J.; van Harten, E. J.; Dupont, D.; La Porta, A.; Tim Prins, P.; Tessier, M. D.; Versteegh, M. A. M.; Zwiller, V.; Bals, S.; Hens, Z.; Rabouw, F. T.; Christianen, P. C. M.; Donega, C. d. M.; Vanmaekelbergh, D. Exciton Fine Structure and Lattice Dynamics in InP/ZnSe Core/Shell Quantum Dots. *ACS Photonics* **2018**, *5*, 3353−3362.

https://doi.org/10.1021/acsnano.1c03864
ACS Nano 2021, 15, 14444−14452

(48) Brovelli, S.; Schaller, R. D.; Crooker, S. A.; Garcia-Santamaria, F.; Chen, Y.; Viswanatha, R.; Hollingsworth, J. A.; Htoon, H.; Klimov, V. I. Nano-Engineered Electron-Hole Exchange Interaction Controls Exciton Dynamics in Core-Shell Semiconductor Nanocrystals. *Nat. Commun.* **2011**, *2*, 280.
(49) Donega, C. d. M.; Bode, M.; Meijerink, A. Size- and Temperature-Dependence of Exciton Lifetimes in CdSe Quantum Dots. *Phys. Rev. B: Condens. Matter Mater. Phys.* **2006**, *74*, 085320.
(50) Norris, D. J.; Efros, Al. L.; Rosen, M.; Bawendi, M. G. Size Dependence of Exciton Fine Structure in CdSe Quantum Dots. *Phys. Rev. B: Condens. Matter Mater. Phys.* **1996**, *53*, 16347−16354.
(51) Woggon, U.; Gindele, F.; Wind, O.; Klingshirn, C. Exchange Interaction and Phonon Confinement in CdSe Quantum Dots. *Phys. Rev. B: Condens. Matter Mater. Phys.* **1996**, *54*, 1506−1509.
(52) Lamb, H. On the Vibrations of an Elastic Sphere. *Proc. London Math Soc.* **1881**, *s1−13*, 189.
(53) Gupalov, S. V.; Merkulov, I. A. Theory of Raman Light Scattering by Nanocrystal Acoustic Vibrations. *Phys. Solid State* **1999**, *41*, 1349−1358.
(54) Saviot, L.; Champagnon, B.; Duval, E.; Kudriavtsev, I. A.; Ekimov, A. I. Size Dependence of Acoustic and Optical Vibrational Modes of CdSe Nanocrystals in Glasses. *J. Non-Cryst. Solids* **1996**, *197*, 238−246.
(55) Sirenko, A. A.; Belitsky, V. I.; Ruf, T.; Cardona, M.; Ekimov, A. I.; Trallero-Giner, C. Spin-Flip and Acoustic-Phonon Raman Scattering in CdS Nanocrystals. *Phys. Rev. B: Condens. Matter Mater. Phys.* **1998**, *58*, 2077−2087.
(56) Salvador, M. R.; Graham, M. W.; Scholes, G. D. Exciton-Phonon Coupling and Disorder in the Excited States of CdSe Colloidal Quantum Dots. *J. Chem. Phys.* **2006**, *125*, 184709.
(57) Chilla, G.; Kipp, T.; Menke, T.; Heitmann, D.; Nikolic, M.; Frömsdorf, A.; Kornowski, A.; Förster, S.; Weller, H. Direct Observation of Confined Acoustic Phonons in the Photoluminescence Spectra of a Single CdSe-CdS-ZnS Core-Shell-Shell Nanocrystal. *Phys. Rev. Lett.* **2008**, *100*, 057403.
(58) Mork, A. J.; Lee, E. M. Y.; Dahod, N. S.; Willard, A. P.; Tisdale, W. A. Modulation of Low-Frequency Acoustic Vibrations in Semiconductor Nanocrystals through Choice of Surface Ligand. *J. Phys. Chem. Lett.* **2016**, *7*, 4213−4216.
(59) Furis, M.; Htoon, H.; Petruska, M. A.; Klimov, V. I.; Barrick, T.; Crooker, S. A. Bright-Exciton Fine Structure and Anisotropic Exchange in CdSe Nanocrystal Quantum Dots. *Phys. Rev. B: Condens. Matter Mater. Phys.* **2006**, *73*, 241313.
(60) Hannah, D. C.; Dunn, N. J.; Ithurria, S.; Talapin, D. V.; Chen, L. X.; Pelton, M.; Schatz, G. C.; Schaller, R. D. Observation of Size-Dependent Thermalization in CdSe Nanocrystals Using Time-Resolved Photoluminescence Spectroscopy. *Phys. Rev. Lett.* **2011**, *107*, 177403.
(61) Rodina, A.; Efros, A. L. Radiative Recombination From Dark Exciton in Nanocrystals: Activation Mechanisms and Polarization Properties. *Phys. Rev. B: Condens. Matter Mater. Phys.* **2016**, *93*, 155427.
(62) Granados del Águila, A.; Jha, B.; Pietra, F.; Groeneveld, E.; Donegá, C. d. M.; Maan, J. C.; Vanmaekelbergh, D.; Christianen, P. C. M. Observation of the Full Exciton and Phonon Fine Structure in CdSe/CdS Dot-in-Rod Heteronanocrystals. *ACS Nano* **2014**, *8*, 5921.

https://doi.org/10.1021/acsnano.1c03864
ACS Nano 2021, 15, 14444−14452